Protein Science (1999), *8*:562–572. Cambridge University Press. Printed in the USA.

Structure in the channel forming domain of colicin E1 bound to membranes: The 402–424 sequence

ŁUKASZ SALWIŃSKI[1] AND WAYNE L. HUBBELL

Jules Stein Eye Institute and Department of Chemistry and Biochemistry, University of California, Los Angeles, Los Angeles, California 90095-7008

(RECEIVED July 9, 1998; ACCEPTED November 5, 1998)

Abstract

To explore the structure of the pore-forming fragment of colicin E1 in membranes, a series of 23 consecutive single cysteine substitution mutants was prepared in the sequence 402–424. Each mutant was reacted with a sulfhydryl-specific reagent to generate a nitroxide labeled side chain, and the mobility of the side chain and its accessibility to collision with paramagnetic reagents was determined from the electron paramagnetic resonance spectrum. Individual values of these quantities were used to identify tertiary contact sites and the nature of the surrounding solvent, while their periodic dependence on sequence position was used to identify secondary structure. In solution, the data revealed a regular helix of 11 residues in the region 406–416, consistent with helix IV of the crystal structure. Upon binding to negatively charged membranes at pH 4.0, helix IV apparently grows to a length of 19 residues, extending from 402–420. One face of the helix is solvated by the lipid bilayer, and the other by an environment of a polar nature. Surprisingly, a conserved charged pair, D408–R409, is located on the lipid-exposed face. Evidence is presented to suggest a transmembrane orientation of this new helix, although other topographies may exist in equilibrium.

Keywords: colicin; membrane protein; nitroxide; site-directed spin labeling

The channel-forming colicins (A, B, E1, Ia, Ib, and N) are bacteriocins that kill sensitive bacterial strains by the formation of voltage-gated ion channels in the cytoplasmic membrane of the target cells. The functional mechanism of killing involves three distinct steps: binding of the toxin to a surface receptor, translocation across the outer membrane, and the insertion of a portion of the toxin in the cytoplasmic membrane to form the ion channel. These three steps are reflected in the tripartate structure of the toxin: the N-terminal domain mediates translocation of the toxin across the outer membrane, the central domain is responsible for receptor binding, and the C-terminal domain is responsible for ion channel formation. Whereas all three domains are required for the toxic activity in vivo, the isolated C-terminal domain retains its channel-forming properties (Dankert et al., 1982) and can be used for in vitro studies of pore formation.

The crystal structure of the soluble form of the entire colicin Ia molecule (Wiener et al., 1997) and of the isolated channel-forming domains of colicins A (Parker et al., 1992), E1 (Elkins et al., 1997), and N (Vetter et al., 1998) have been reported. In all three cases the pore forming domain is composed of 10 α-helices arranged in three layers. Two of the helices of the central layer, composed almost exclusively of hydrophobic residues, form a hairpin buried within the protein interior. The remaining eight amphipathic helices surround this hydrophobic core and protect it from the contact with solvent (Fig. 1A).

Low pH triggers the insertion of the C-terminal domain into phospholipid bilayers, a process accompanied by a conformational change that can be detected at the level of both secondary and tertiary structure (Zakharov et al., 1998). An increasing body of evidence suggests that the hydrophobic hairpin spans the membrane (Song et al., 1991; Kienker et al., 1997; Kim et al., 1998; Lambotte et al., 1998), whereas the remaining amphipathic helices are thought to be spread out on the membrane surface (Parker et al., 1992; Zhang & Cramer, 1992; Elkins et al., 1997; Zakharov et al., 1998). The structure of the protein undergoes further changes upon application of a transmembrane potential, and additional regions of the protein are inserted into the lipid bilayer to form an open, functional channel (Merrill & Cramer, 1990; Slatin et al., 1994; Qiu et al., 1996).

Reprint requests to: Wayne L. Hubbell, Jules Stein Eye Institute, UCLA School of Medicine, Los Angeles, California 90095-7008; e-mail: hubbellw@wlheye.jsei.ucla.edu.

[1]Present address: UCLA-DOE Laboratory of Structural Biology and Molecular Medicine, University of California, Los Angeles, Los Angeles, California 90095-1570.

Abbreviations: EPR, electron paramagnetic resonance; SDSL, site-directed spin labeling; NiEDDA, Ni(II)ethylenediaminediacetate; NiAA, Ni(II) acetonylacetone; β-ME, β-mercaptoethanol; MES, 2-(4-morpholino)-ethane sulfonic acid; MOPS, morpholinopropane sulfonic acid; EDTA, ethylenediaminotetraacetic acid; DTT, dithiothreitol; SLPC-n, palmitoyl-stearoyl *n*-(2,2-dimethyloxazolidinyl-1-oxy)-phosphatidylcholine (n = 7, 10, 12); POPC, palmitoyl-oleoyl-phosphatidylserine; POPG, palmitoyl-oleoyl-phosphatidylglycerol; TPX, polymethylpentene; T4L, T4 lysozyme.

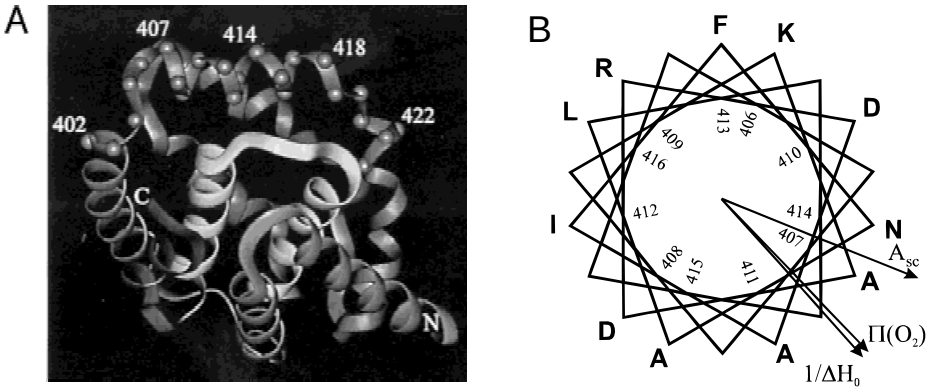

Fig. 1. A: Crystal structure of the colicin E1 tryptic fragment showing the location of residues 402–424. **B:** Helical wheel representation of the 406–416 sequence, corresponding to Helix IV in the crystal structure. The arrows indicate the direction of the moments (Eisenberg et al., 1984) for $\Pi(O_2)$, ΔH_0^{-1}, and A_{sc}, the solvent accessible surface area (Bowie et al., 1991) calculated from the crystal structure for an alanine residue substituted at the indicated position.

In spite of the wealth of biochemical and functional data (see Cramer et al., 1995; Stroud, 1995 for recent reviews), the structures of the membrane bound forms of colicins remain largely unknown. Apart from the hydrophobic hairpin believed to span the thickness of the membrane, neither the extent nor membrane localization of other secondary structure elements have been established. The crystal structures of the soluble forms of the channel-forming domains provide little insight into possible membrane-bound structures, other than the necessity of a secondary structure rearrangement, because the majority of helices observed are too short to span a lipid bilayer.

The goal of the current study is to examine the secondary structure and membrane topology of the 402–424 region in the C-terminal domain of colicin E1. This sequence lies adjacent to the segment that is apparently inserted into the lipid bilayer during voltage-gating (Merrill & Cramer, 1990), and within the larger domain believed to be translocated across the membrane during channel formation in the homologous colicin Ia (Slatin et al., 1994; Qiu et al., 1996).

The experimental approach is SDSL, which has proven effective in analyzing structural and dynamic features of both soluble and membrane-bound proteins of arbitrary size (for recent reviews see Hubbell & Altenbach, 1994; Feix & Klug, 1998; Hubbell et al., 1998). The strategy is based on the introduction of a single cysteine residue into a cysteine-less background, followed by modification of the unique sulfhydryl with a selective nitroxide reagent. In the present studies the methanethiosulfonate reagent (I) is employed to introduce the nitroxide side chain designated R1.

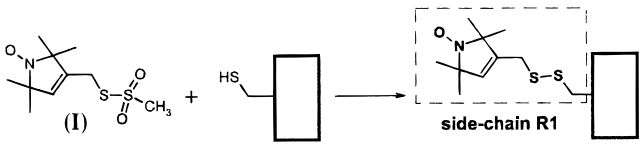

Two features are derived from the EPR spectra of R1 that characterize the protein structure: (1) the mobility of the nitroxide and (2) the accessibility of the nitroxide to collisions (Heisenberg exchange) with paramagnetic reagents in solution.

The term "mobility" is a qualitative descriptor of the motional state of the nitroxide, and includes both frequency and amplitude effects as reflected in the breadth of EPR spectral features. At X-band microwave frequencies, the spectrum of the nitroxide is highly sensitive to motion characterized by correlation times in the range 10^{-8}–10^{-11} s. The upper limit in this range approximately corresponds to rotational correlation times of proteins around 20 kD, such as the C-terminal fragment of colicin E1 studied here ($\tau \approx 8$ ns). Hence, the EPR spectra will reflect rotational motion of the protein as a whole in addition to the motion of the side chain relative to the protein. To eliminate effects from the rotational motion of the protein, the viscosity of the solution is increased by the addition of sucrose or glycerol (Mchaourab et al., 1996).

In principle, a detailed motional model for the side chain can be deduced by simulation of the EPR spectrum (Freed, 1989; Timofeev & Samarianov, 1993). However, in the absence of sufficient experimental constraints, the large number of parameters involved limit the utility of this approach at the present time. As an alternative, the inverse spectral second moment ($\langle H^2 \rangle^{-1}$) and the inverse central linewidth (ΔH_0^{-1}) are used as coarse measures of side-chain mobility (Mchaourab et al., 1996). In a comprehensive study in T4L, it was shown that side-chain mobility measured by these parameters alone is often sufficient to classify a site as belonging to one of four topographical categories: solvent-exposed helix surface sites, loop sites, buried sites, or tertiary contact sites (Mchaourab et al., 1996).

The accessibility of an R1 side chain to collisions with a paramagnetic reagent is directly related to the solvent accessibility of side chain, and is measured by the experimental "accessibility parameter," Π, determined from the shift in spin lattice relaxation time of the nitroxide (Farahbakhsh et al., 1992). For membrane proteins, both polar and nonpolar paramagnetic reagents are needed to explore the side-chain topography. Metal ion complexes such as NiEDDA, NiAA, and chromium (III) oxalate are common choices for a polar reagent insoluble in the membrane interior, while O_2 is the preferred choice as a relatively nonpolar reagent, soluble both in water and the membrane interior.

Systematic "nitroxide scanning" experiments yield sequence-correlated side-chain mobility and accessibility data that can be interpreted in terms of both secondary and tertiary structure. For example, periodic variation in mobility or Π along a sequence can serve to identify regular secondary structure, and both α-helical and β structures have been analyzed (Hubbell et al., 1996). In

addition, the orientation of the structure in the protein can be determined, because the surface facing the solvent has the highest mobility and solvent accessibility.

For membrane proteins, analysis of the relative accessibility of the R1 side chain to polar and nonpolar reagents reveals additional information on protein topography. For example, a helical segment adsorbed on the surface of a membrane will show a periodic dependence of Π with sequence position for both polar and nonpolar reagents due to differential solubilities in the membrane and aqueous phases. However, the periodic functions will be 180° out of phase. This situation is diagnostic for asymmetric solvation of a periodic structure (Oh et al., 1996). In addition, differential accessibilities to polar and nonpolar reagents may be used to determine the depth of immersion of a labeled site in the membrane (Altenbach et al., 1994). Within the membrane interior, Π values for both polar and nonpolar reagents depend on the depth of the nitroxide from the membrane/aqueous interface as a result of gradients in the concentration-diffusion coefficient product along the membrane normal. In studies on bacteriorhodopsin and spin-labeled phospholipids, it has been found that the quantity Φ,

$$\Phi = \ln\left(\frac{\Pi(O_2)}{\Pi(\text{polar})}\right) \quad (1)$$

is a linear function of depth in the membrane, measured from the nearest membrane/aqueous interface. Thus,

$$d = a\Phi + b \quad (2)$$

where d is the depth in angstroms, and a and b are constants to be determined from an appropriate calibration. This relationship has been verified for both NiAA and NiEDDA as polar reagents (Altenbach et al., 1994).

In the present work, the mobility, $\Pi(\text{NiEDDA})$, and $\Pi(O_2)$ have been determined for an R1 side chain introduced at each site from 402 to 424 in the C-terminal domain of colicin E1, both in solution and the membrane bound state. Analysis of the periodicity of mobility and P values along the sequence in solution reveals a well-defined helical structure from 406–416, in close agreement with the crystal structure. In the membrane-bound state, a continuous helical structure extends from 402–420, representing an increase in helical length by eight residues. Moreover, an out-of-phase periodicity in $\Pi(\text{NiEDDA})$ and $\Pi(O_2)$ indicates asymmetric solvation of the helical segment in the membrane. Finally, the dependence of Φ on sequence position suggests a transmembrane orientation of the elongated helical segment.

Results

Protein expression and labeling

All single cysteine mutants in the 402–424 series were expressed at a level of 25–40 mg of protein/liter of culture, and purified to 95–99% homogeneity as determined by SDS-PAGE. All mutants were active to at least 5^4x dilution of a $OD_{280} = 0.1$ stock solution as determined by an in vivo activity test (Table 1).

Trypsin digestion of the colicin E1 mutants resulted in a fragment smaller than previously reported, presumably due to differences in the digestion conditions. By sequencing 5–6 residues of its N-terminus, the product was identified as starting at position 347, rather than at position 336 as reported earlier (Dankert et al., 1982). No contamination of the tryptic fragment was detected by SDS-PAGE after the final cation-exchange purification step. Reaction of the unique cysteine in each purified fragment with the methanethiosulfonate (I) was essentially quantitative. No reaction was detected with the cysteine-less derivative.

Table 1. *In vivo activity of colicin E1 single cysteine mutants*

Mutant	Dilution from $OD_{280} = 0.1$[a]			
K402C	+	+/−	−	−
K403C	+	+/−	−	−
F404C	+	+	−	−
S405C	+	+	+/−	−
K406C	+	+	−	−
A407C	+	+	−	−
D408C	+	+	−	−
D408C[b]	+	−	−	−
R409C	+	+/−	−	−
R409C[c]	+	+/−	−	−
D410C	+	+	−	−
A411C	+	+	−	−
I412C	+	+	−	−
F413C	+	+	−	−
N414C	+	+	+	−
A415C	+	+	+	−
L416C	+	+	+	−
A417C	+	+	+	+
S418C	+	+	+	−
V419C	+	+	+	−
K420C	+	+	+	−
Y421C	+	+	+	−
D422C	+	+	+	−
D423C	+	+	+	−
W424C	+	+	+	−

[a] Activity measured as described in Materials and methods. +, Positive activity—a clear no-growth zone around the filter; +/−, intermediate activity—distinct but opaque zone around the filter; −, no activity.
[b] D408C, R409S charge compensation mutant.
[c] R409C, D408S charge compensation mutant.

Structure of the 402–424 sequence in solution

The location of the 402–424 sequence in the crystal structure of colicin E1 is shown in Figure 1A. The EPR spectra of colicin E1 in solution and its C-terminal fragment bearing R1 residues at each of these sites are shown in Figures 2 and 3, respectively. Sharp features visible in some spectra of the intact colicin E1 (Fig. 2, arrows) correspond to 1–5% background spin label population attached to a contaminating protein. Those features are virtually nonexistent in the spectra of the tryptic fragment, consistent with its higher degree of purity.

Apart from the sharp component, the spectra of the intact colicin E1 molecule are generally broader than their fragment counterparts (Fig. 3). The difference between the spectra, reflecting increased mobility of the spin label attached to the tryptic fragment, could be a result of a change in the domain structure after trypsin digestion, or simply a consequence of the reduction in protein size and concomitant decrease in the rotational correlation time (τ_R). In the intact molecule (MW = 56 kD), rotational diffusion is slow, and

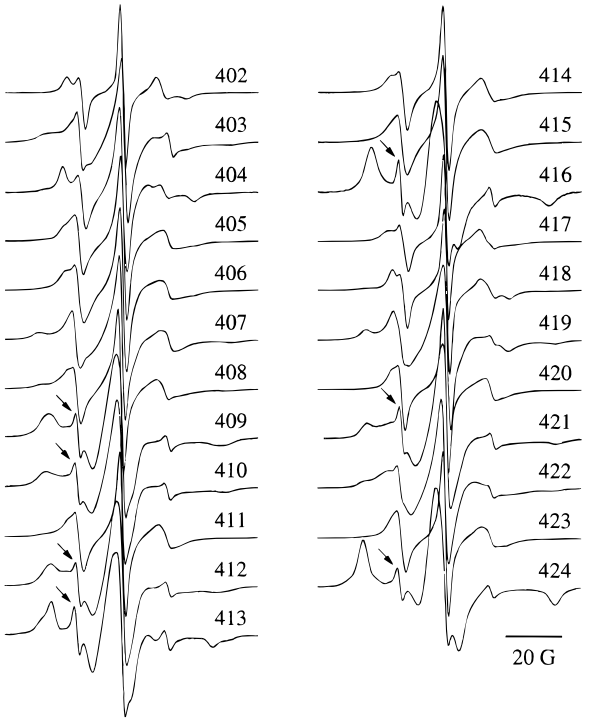

Fig. 2. EPR spectra of intact colicin E1 bearing the nitroxide side chain R1 at the indicated positions. Spectra were recorded at ambient temperature in HS buffer (see Materials and methods) at protein concentrations between 100 and 300 μM. The sharp features visible in some spectra (arrows) are the result of a small amounts of contaminating proteins.

does not average the nitroxide magnetic anisotropies. Hence the EPR spectra reflect motion of the side chain relative to the protein. However, for the fragment (MW = 20 kD) in water, $\tau_R \approx 8$ ns and rotational diffusion has a significant contribution to spectral averaging. Rotational diffusion effects can be reduced by recording the spectra of spin labeled fragments in 38% (w/w) sucrose, where $\tau_R \approx 40$ ns, out of the range of maximum sensitivity of lineshape to motion. Figure 4 compares representative spectra of spin-labeled intact molecules in water with the corresponding tryptic fragment in 38% sucrose. As can be seen, the increased viscosity compensates for the decrease of the size of the protein molecule, and restores the line shapes to those of the intact molecule. This result indicates that the structure of the C-terminal fragment in the sequence 402–424 remains intact after trypsin digestion. Moreover, the similarity of the spectra of the intact molecule in water and the fragment in high viscosity suggests that direct contacts between the C-terminal domain and other parts of the protein, if present, are limited to regions outside of the 402–424 segment. Otherwise, changes in side-chain mobility should be detected due to the elimination of contact interactions.

Analysis of R1 side-chain accessibility leads to similar conclusions. As shown in Figure 5B, the pattern of $\Pi(O_2)$ for the intact molecule (open symbols) and tryptic fragment (solid symbols) is similar, with significant differences only in the region 421–423, indicating again that the overall structure of the C-terminal fragment is similar in the two cases. The differences in collision rates, but not in line shape observed in 421–423 may indicate that another part of the protein, removed by proteolysis, is nearby but not in contact with these residues in the intact molecule.

Variations of R1 mobility and *P* values between individual sites reflect differences in the local environment at the labeled sites. Figure 5 shows the sequence dependence of R1 mobility (measured by ΔH_0^{-1}) and Π(NiEDDA) in addition to $\Pi(O_2)$ in the region 402–424. As is evident, there are in-phase oscillations in all three quantities in the range 406–416 that are well described by a function of period 3.6, suggesting that the region is α-helical. R1 residues at 409, 412, 413, and 416 have low mobility, low $\Pi(O_2)$, and low Π(NiEDDA) values indicating that they reside on the face of the helix buried within the protein interior (Mchaourab et al., 1996). R1 residues at 407, 411, 414, and 415 have a high mobility with spectral line shapes indicative of solvent-exposed helical sites (Mchaourab et al., 1996), and *P* values consistent with solvent-exposed sites (Hubbell et al., 1996). R1 at site 407 has a distinctive two-component lineshape similar to that observed at N-terminal helical locations, and R1 at other sites in the sequence have intermediate values of mobility and accessibility indicating sites of tertiary interactions (Mchaourab et al., 1996).

The periodic pattern is broken outside of the 406–416 stretch, effectively setting limits on the extent of the regular helix. However, this could be an overestimation of the actual helix length as defined by a more strict backbone hydrogen bonding pattern and Ψ,Φ angle criteria, and the helix could be shorter by 1 or 2 residues at each end.

Spin labels attached to sites directly flanking the 406–416 helix, especially at positions 417, 418, and 420, have high mobility (Figs. 2, 5B) and relatively high exposure to both NiEDDA and O_2 (Fig. 5B,C), indicating that they are localized within a less ordered, solvent exposed region possibly corresponding to an interhelical loop. R1 side chains within the four-residue stretch 421–

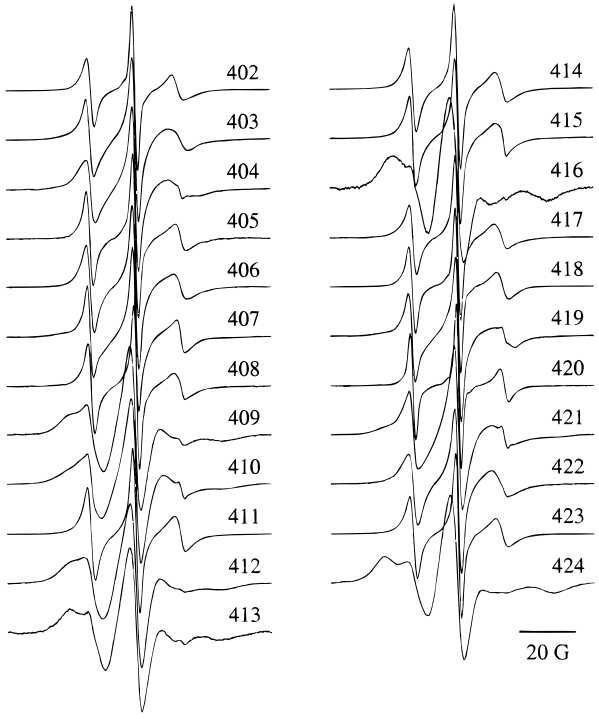

Fig. 3. EPR spectra of the tryptic fragment of colicin E1 bearing the nitroxide side chain R1 at the indicated positions. Spectra were recorded under the same conditions as in Figure 2.

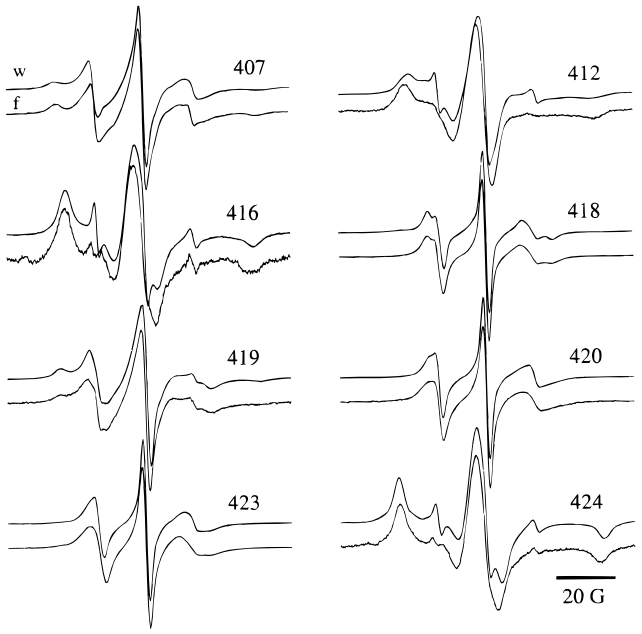

Fig. 4. Comparison of the EPR spectra of the indicated spin-labeled colicin E1 fragments in 38% (w/w) sucrose in HS buffer (lower traces), and the corresponding spectra of the intact protein in the same buffer (upper traces). Protein concentrations were between 100 and 300 μM.

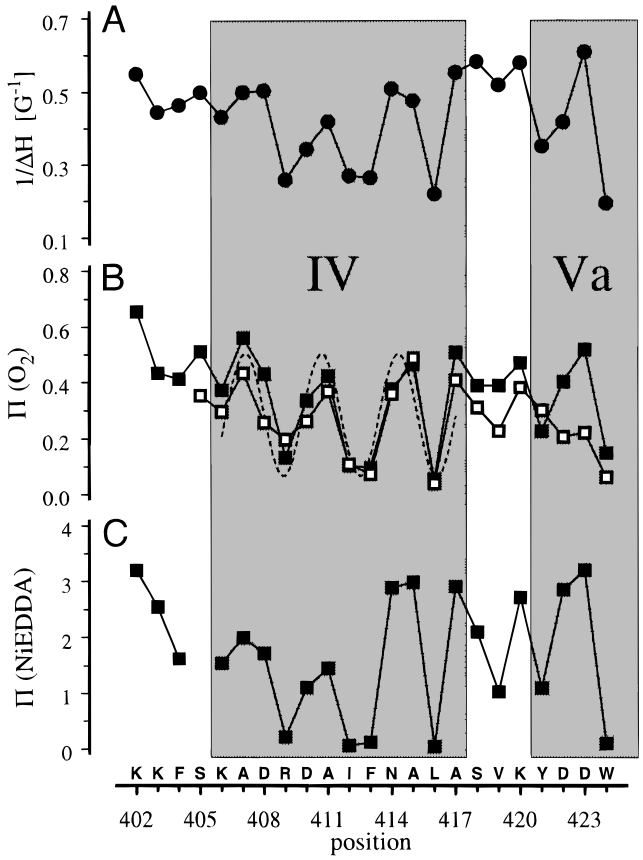

Fig. 5. Mobility and accessibility of the R1 side chain as a function of sequence position in the region 402–424 for colicin E1 in solution. The shaded zones mark the locations of Helices IV and Va observed in the crystal structure. **A:** Mobility as measured by the inverse central line width (ΔH_0^{-1}). **B:** $\Pi(O_2)$ for colicin in HS buffer in equilibrium with air. The solid symbols (■) are for the trypic fragment and the open symbols (□) for the intact molecule. The dashed line is a function of period 3.6 in residue position. **C:** Π(NiEDDA) for NiEDDA at 10 mM in HS buffer.

424 also have properties periodic in sequence position that might suggest the beginning of another helical segment, but the region is too short to permit a definitive conclusion.

An examination of Figure 1 reveals that the above interpretation of the spin labeling data from colicin E1 in solution is in excellent agreement with the crystal structure (Elkins et al., 1997). In that structure, an α-helix (Helix IV) extends from 406–416, coinciding with the assignment based on the periodicity in Π values and side-chain mobility for the fragment in solution. The orientation of the helical segment within the structure is defined by the direction of the $\Pi(O_2)$ (or Π(NiEDDA)) and ΔH_0^{-1} moments shown in Figure 1B. These vectors point in the direction of maximum accessibility and mobility, and identify the solvent exposed surface of the helix. As seen in Figure 2B, these moments point to the same face of the helix as the moment of side-chain solvent accessibility A_{sc} computed from the crystal structure (see Fig. 1 caption). The small angular difference of $\sim$20° between A_{sc} and $\Pi(O_2)$ moments could be due to a difference between the structure in the crystal and solution, but could also be a result of the conformational flexibility of the R1 side chain.

Structure in the membrane-bound state at pH 4

Figure 6 shows the EPR spectra of the spin labeled colicin E1 tryptic fragment bound to phospholipid vesicles at pH 4. To appreciate the dramatic structural changes from the solution state, these spectra should be compared with those for the intact colicin E1 of Figure 2, which are equivalent to the spectra of the tryptic fragment in the absence of rotational motion of the protein. This is a valid comparison, because the membrane bound species has very slow rotational diffusion. R1 residues at 409, 412, and 416, which are immobilized due to strong interactions within the core of the soluble protein, now have spectra reflecting a high mobility, consistent with sites on the exposed surface of an α-helix (Mchaourab et al., 1996). On the other hand, mobile R1 residues at 405, 415, 417, and 423, located at solvent exposed sites in the solution structure, have drastically reduced mobility. This pattern of mobility changes suggests an effective inversion of the local structure upon membrane binding.

Figure 7 shows the variation of $\Pi(O_2)$ and Π(NiEDDA) with sequence position in the membrane bound state in the region 402–424. Although the dynamic range of the values is smaller than those in the solution structure, there is a discernable periodic variation in both $\Pi(O_2)$ and Π(NiEDDA) that extends from approximately 402 to 420, suggesting a structure with the period of an α-helix. If this is indeed the case, the helix length increases by at least two turns upon membrane binding. Moreover, oscillations in $\Pi(O_2)$ and Π(NiEDDA) are approximately 180° out of phase, characteristic of an asymmetrically solvated structure localized at a water-lipid interface (Oh et al., 1996). This is to be compared with the solution structure, where $\Pi(O_2)$ and Π(NiEDDA) are in phase with one another (Fig. 5B,C), as expected for a protein molecule surrounded by a single, homogeneous solvent.

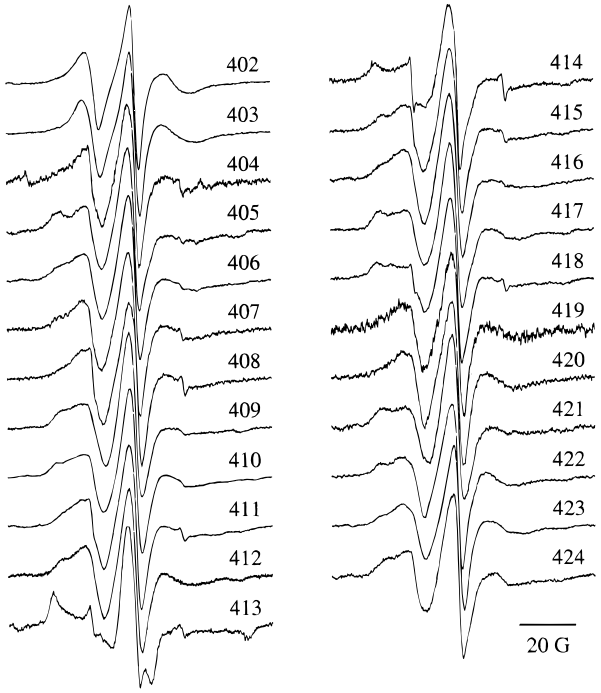

Fig. 6. EPR spectra of spin labeled colicin E1 tryptic fragment bound to POPC:POPG (2:1 w/w) vesicles (pH = 4.0) at room temperature.

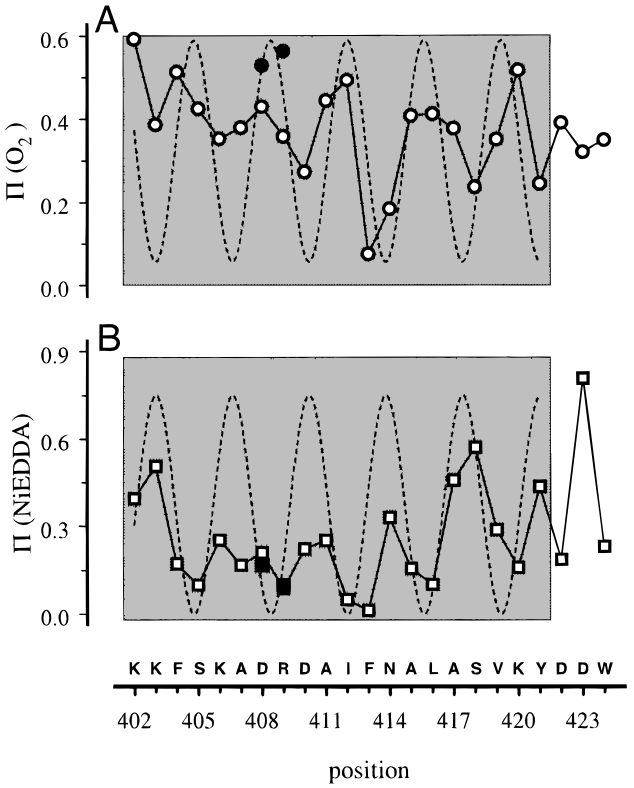

Fig. 7. Accessibility of the R1 side chain as a function of position in the sequence 402–424 for membrane-bound colicin E1 tryptic fragment at pH 4. **A:** $\Pi(O_2)$—the concentration of O_2 was that in equilibrium with air. **B:** Π(NiEDDA)—the concentration of NiEDDA was 150 mM. Closed symbols denote charge-compensated mutants D408R1/R409S and D408S/R409R1.

The periodicity throughout the 402–420 sequence in the membrane-bound state is more clearly illustrated by the Φ function (Equation 1), which enhances the contrast between $\Pi(O_2)$ and Π(NiEDDA), and partially corrects for local structural effects, which modulate the Π values (Altenbach et al., 1994). Φ is largest for sites with a higher accessibility to O_2 compared with NiEDDA. A plot of Φ vs. sequence position is shown in Figure 8A, where the helix periodicity is easily recognized. The local maxima and minima in Φ identify the lipid exposed and aqueous exposed surfaces of the helix, respectively. Indeed, when the sequence is mapped on a helical wheel representation (Fig. 8B), the residues apparently most exposed to lipid (402, 405, 409, 412, 416, and 420) are closely grouped on one face of the putative helix. The mobility of R1 side chains at these sites is relatively high (Fig. 6), consistent with a location on the exposed surface of a helix (Mchaourab et al., 1996). Surprisingly, the predicted lipid-exposed face is quite polar, with the positively charged residue R409 directly facing the hydrophobic interior of the bilayer, and K402 and K420, at the termini of the helix, at one edge. As discussed below, the residues D408 and R409 may form an ion pair in the bilayer.

Sites localized on the face of the helix pointing away from the lipid bilayer have various levels of spin label immobilization and limited collisions with both oxygen and NiEDDA, indicating that this surface remains in contact with other parts of the molecule. However, the presence of relatively mobile R1 side chains on this face (403, 404, 407, 408, 411, and 415) suggest a loose protein–protein packing with cavities that permit motion of the side chains. These cavities are likely to be solvated by water, judging from the relatively high accessibility to NiEDDA compared to O_2, a situation giving rise to the out-of-phase periodicity in these quantities.

Two alternative arrangements of the helix might account for the data. The helix could lie parallel to the membrane surface, with one face directly exposed to the bilayer interior and the opposing face in contact with other parts of the protein at the aqueous/bilayer interface. Alternatively, the helix may span the membrane thickness with one surface directed toward the bilayer interior and the other involved in limited protein–protein contacts and in at least partial contact with solvent.

To distinguish between these possible topologies, the immersion depth of the residues exposed on the hydrophobic face of the helix was estimated from the Φ function (Altenbach et al., 1994). The calibration curve ($d = 5.5\Phi + 8.1$) was obtained with the use of phospholipids spin-labeled at different positions along the hydrocarbon chain in bilayers containing colicin (see Materials and methods). Only residues on the exposed surface of the helix are used for depth estimation to eliminate steric exclusion effects due to the difference in size between O_2 and NiEDDA (Altenbach et al., 1994). For an α-helix lying on the surface, the lipid exposed residues are predicted to vary in depth from site-to-site, but not in a regular fashion. For a transmembrane configuration, successive lipid-exposed residues along the sequence should show a regular increase in depth from the membrane/aqueous interface to the center of the bilayer, and then decrease in depth to the opposing bilayer surface. As shown in Figure 8A, the immersion depth for the most exposed residues (maxima in the Φ function, solid circles) is greatest for R1 at 412, and decreases in a roughly linear fashion (dashed line), as predicted by Equation 2, when R1 is moved in

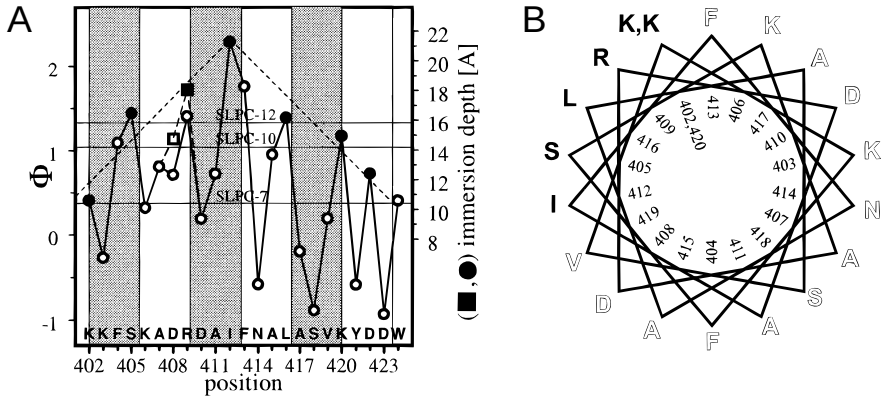

Fig. 8. A: Φ as a function of R1 position in the sequence 402–424 for membrane-bound colicin E1 tryptic fragment at pH 4. Φ was computed from the data of Figure 7, and the immersion depth was computed as described in the text. Solid symbols identify local maxima in Φ that were used for immersion depth calculations. Horizontal lines marked SLPC-7, SLPC-10, and SLPC-12 indicate the depths of the nitroxides in these reference spin-labeled phosphatidylcholine lipids (see Materials and methods). The width of the vertical bars (3.6 residues) corresponds to α-helix periodicity. **B:** A helical wheel representation of the 402–420 sequence. Black letters indicate residues corresponding to maxima in Φ function. The square symbols refer to data obtained with the corresponding charge-compensated mutant (see text).

either direction along the helix. Residue 412 is at a depth consistent with the center of the bilayer. Note that R1 residues at 422 and 424 also fall on the regular depth progression, although these residues are not formally part of the helical structure. However, nitroxides at these sites are mobile and face the lipid bilayer, and the depth measurement is expected to be valid. Among the lipid exposed residues, R409R1 is shallower than expected. Introduction of a spin label at this site is accompanied by removal of only one of the charges involved in the formation of a putative salt bridge between D408 and R409. As a result, an isolated, potentially charged, glutamate residue is created on the lipid-exposed face of the helix. Although at pH 4.0 the energetic cost of neutralizing this residue by protonation is relatively low, its presence may effect the position of the helix in the bilayer. To examine this potential source of labeling artifact, D408S/R409R1, lacking both charges, was examined. Introduction of the additional mutation resulted in a decrease of the trypsin resistance of the C-terminal fragment, but no change of the solution EPR spectral line shape relative to R409R1 was observed (data not shown), indicating that the additional mutation had little or no effect on the protein fold in solution around the labeled site.

The EPR spectrum of the membrane bound form of D408S/R409R1 shows a significant decrease in the population of a more immobilized component relative to that of R409R1 alone (Fig. 9A), showing that removal of the glutamate at 408 results in structural rearrangement of the protein in the vicinity of the labeled site. As shown in Figure 7 (solid symbols), the nitroxide in the charge-compensated mutant D408S/R409R1 shows an increase in accessibility to O_2, but no measurable difference in accessibility to NiEDDA relative to R409R1 alone. The observed change in $\Pi(O_2)$ is in the direction expected for a deeper location in the bilayer for the nitroxide in the charge-compensated double mutant. It is not obvious why there is no difference in the accessibility to NiEDDA between D408S/R409R1 and R409R1, but this could be due to the inherent problem associated with detecting differences in a very small values of P(NiEDDA). Nevertheless, the estimated depth of immersion is greater for the charge compensated mutant, and the value for the lipid-exposed surface residue in D408S/R409R1 now falls more in line with the approximately linear depth-dependent profile of the other lipid-exposed residues (solid square, Fig. 8A).

The mutation D408R1 also leaves a net charge (409R) that would be expected to effect the position of the putative helix in the membrane. Although it is not among the set selected for depth estimation, the comparative effect of the charge compensating mutation D408R1/R409S was also examined. The EPR spectrum of D408R1/R409S was essentially identical to that of D408R1 alone in solution (data not shown) and in the membrane bound state (Fig. 9B). However, the accessibility to O_2 and NiEDDA increased and decreased slightly, respectively, relative to D408R1 alone (Fig. 7), consistent with a deeper location in the membrane for the charge-compensated double mutant (Fig. 8, solid symbols).

pH-Dependent structure in the membrane-bound state

Earlier studies reported effects of pH changes attributable to structural rearrangements in membrane-bound colicins (Collarini et al.,

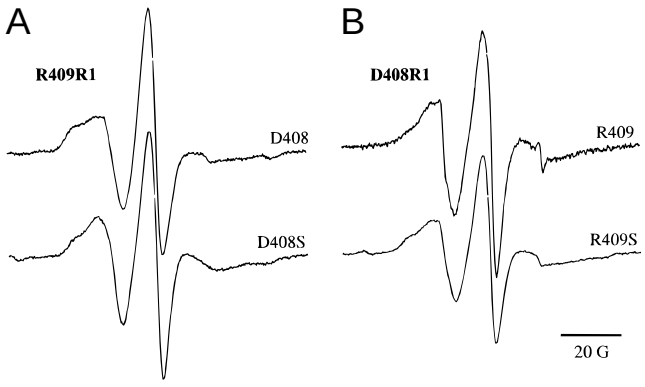

Fig. 9. A comparison of the EPR spectra of (**A**) R409R1, (**B**) D408R1, and the corresponding charge compensated mutants D408R1/R409S, D408S/R409R1 in the membrane bound state of the colicin E1 tryptic fragment at pH = 4.0.

1987; Xu et al., 1988; Geli et al., 1992). To examine this possibility, colicin E1 mutants I412R1 and A417R1 were selected for an initial investigation. Figure 10 shows the EPR spectra of these mutants bound to vesicles at pH = 4.0 and after a pH shift to pH = 7.1. At pH 4.0, the spectrum of the nitroxide in I412R1 reveals two components, consistent with a helix surface site with possible tertiary interaction (Mchaourab et al., 1996). A shift to pH 7.1 results in a decrease in the population of the more mobile component with a concomitant increase in the population of the more immobile component. In A417R1 at pH 4.0, the nitroxide is strongly immobilized due to an interaction with other parts of the protein. A shift to pH 7.1 results in a dramatic increase in the mobility of the nitroxide, indicating that a pH induced conformational change occurs that involves a significant rearrangement of the tertiary fold of the protein. These effects are entirely reversible (data not shown). A detailed study of the pH-dependent conformational switch throughout the 402–424 region will be published elsewhere, but these two examples serve to indicate the existence of pH dependent conformational equilibria in the membrane-bound colicin E1 C-terminal domain.

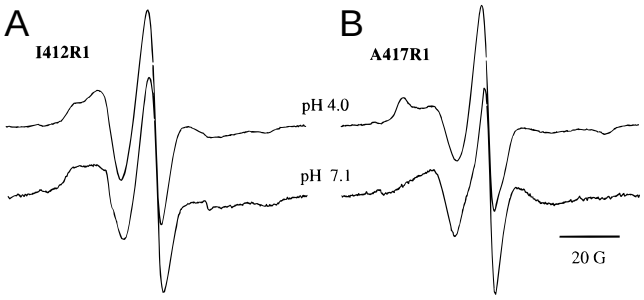

Fig. 10. EPR spectra of membrane bound colicin E1 tryptic fragments (**A**) I412R1 and (**B**) A417R1 at pH 4.0 and pH 7.1.

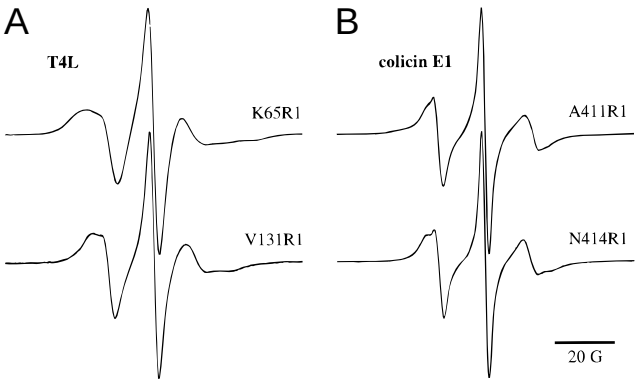

Fig. 11. EPR spectra of R1 at helix surface sites. (**A**) Sites 65 and 131 in T4 lysozyme (Mchaourab et al., 1996); (**B**) sites 411 and 414 in colicin.

Discussion

The SDSL analysis presented above for the C-terminal domain of colicin E1 in solution reveals a structure in the 402–424 region compatible with that of the recently reported crystal structure (Elkins et al., 1997). In particular, the periodic variation of side chain mobility and accessibility to both O_2 and NiEDDA clearly reveals the existence of the regular α-helix in the sequence 406–416 (Fig. 1), corresponding to helix IV in the crystal structure. This result adds to the growing body of evidence from proteins of known structure that the R1 side chain produces little structural perturbation at the level of the backbone fold, and that nitroxide scanning is a viable method for determination of sequence-correlated secondary structure in proteins (Altenbach et al., 1990; Mchaourab et al., 1996; Oh et al., 1996; Klug et al., 1997; Voss et al., 1997; Koteiche et al., 1998; Perozo et al., 1998). Moreover, comparison of data from the intact molecule and the isolated C-terminal domain show the structure of the domain to be similar in the region investigated in both preparations.

Figure 11 compares the EPR spectral line shapes of R1 side chains on solvent-exposed surface sites of Helix IV in colicin E1 (411, 414; Fig. 1) with those of similar sites in T4L (65, 131; Mchaourab et al., 1996). The sites compared are at locations where the nitroxide is unlikely to experience tertiary interactions with other parts of the structures. As can be seen, the EPR spectral line shapes of the R1 side chains in colicin E1 are narrower than those in T4L, suggesting that the mobility of the R1 side chain is higher in colicin, even though site 131 in T4L is located in a short two-turn helix and is among the most mobile of the helix surface sites in that molecule. The difference in mobility between the helix surface sites in T4L and colicin E1 is unlikely to be due to differences in rotational motions of the proteins as a whole, because the mobility of buried sites in the two proteins is similar, based on the line shapes and separation of the outer hyperfine extrema. Rather, the difference is likely to be due to thermal activation of internal modes in the colicin molecule. This is consistent with the suboptimal packing in the colicin E1 tryptic fragment, and the generally higher thermal factors compared to T4L (Alber et al., 1987; Elkins et al., 1997).

Comparison of the data obtained for the soluble and membrane bound forms of the colicin fragment reveals dramatic differences at the levels of both secondary and tertiary structure. For example, Helix IV increases in length from approximately 11 residues in the solution structure to 19 residues in the membrane-bound state to provide a helix sufficiently long to span the hydrophobic thickness of the bilayer. This change is apparently accompanied by concomitant disassembly of Helix Va (residues 421–425; Fig. 1) as suggested by the irregular variation in $\Pi(O_2)$ and Π(NiEDDA) (see Figs. 5, 7). The net result of these transformations is an overall increase in the helicity of the region, consistent with circular dichroism studies that reveal a net increase in helicity of the entire molecule upon membrane association (Zakharov et al., 1998). However, the results presented here show that helices existing in the solution state may be destroyed upon membrane binding, an event that could not be appreciated from the circular dichroism studies.

In the membrane bound state, the helical segment from 402–420 is asymmetrically solvated, with one face in contact with the lipid bilayer, and the remaining surface involved in either protein–protein contacts or directly solvated with water. As noted above, this may result from either of two possible topographies of the helix: one in which the helix lies parallel to the membrane surface, and the other in which the helix is transmembrane. The data of Figure 8 favor a transmembrane orientation, but there is a caveat, namely that the slope of the linear relationship between estimated depth and residue number is approximately 0.8 Å/residue rather than the expected 1.5 Å/residue for a transmembrane helical seg-

ment. One possible explanation is that colicin E1 exists in multiple conformations in equilibrium. For example, an equilibrium between a state with the helix parallel to the membrane and a state with the helix in a transmembrane orientation could give rise to a shallow depth profile of the type observed with the maximum depth near the center of the bilayer. That such an equilibrium could exist is suggested by the reversible pH dependent structural reorganization involving the 402–420 helical segment (Fig. 10). The influence of such equilibria on the apparent depth will be explored in future experiments. Another possibility is a tilted transmembrane helix, but in this configuration, the 402–420 segment would not reach across the thickness of the bilayer.

In any model for the structure consistent with the data, it is surprising that charged residue R409 is localized close to the center of the lipid exposed face. The adjacent residue, D408, may form an ion pair with R409. Complete conservation of charge, but not residue type, is found at these positions in all membrane-associated colicins. The reason for this strict conservation is not obvious in the solution structure, because D408 and R409 residues are not positioned to form a salt bridge with each other or any other residues in the structure. However, in the low dielectric interior of the bilayer, ion-pair formation would be strongly favored. Modeling of residues i and $i + 1$ on a helix surface suggest that a 2–3 Å separated ion pair could be formed with conformations of Arg and Glu side chains that are observed to occur in known protein structures.

The presence of a lipid-exposed salt bridge on a helix surface is not without precedent, and has been observed in a transmembrane helix of the chlorophyll antenna complex between residues at i and $i + 3$ (McDermott et al., 1995). Theoretical estimates of the free energy required for burying an ion pair lie in the range of 10–15 kcal/mol (Honig et al., 1986). However, this unfavorable contribution is offset by the favorable energy of insertion of an entire transmembrane segment, which has been estimated to be as low as −30 kcal/mol (Jahnig, 1983; Engelman et al., 1986). Of course this may be lowered further by interaction of the helix with other parts of the protein. Under any condition, the increase in free energy of helix insertion due to a lipid-exposed ion pair would limit the stability of the transmembrane conformation, a feature essential for reversible molecular gating under the influence of transmembrane potential (Slatin et al., 1994).

Despite the large energetic consequences associated with introduction of charged residues on the lipid-exposed surface of transmembrane helices, only small differences in local structure, depth of immersion, and functional activity (Table 1) were observed between R409R1 and the charge compensated mutation D408S/R409R1. As noted above, this may be due to the relatively low free energy associated with neutralization of D408 by protonation at pH 4.0 (≈1–2 kcal/mol for 90% protonation). Similarly, relatively small differences in local structure and functional activity were noted between D408R1 that leaves an isolate Arg residue at 409, and the charge compensated mutation D408R1/R409S. In this case, neutralization of the Arg by deprotonation at pH 4.0 is high (≈14 kcal/mol for 90% deprotonation), and large effects on structure and function would be expected in the D408R1 mutant. A possible explanation for the absence of such effects is the presence of a Glu residue at position 410, which may form an alternate ion pair with R409 in the absence of D408.

The charged residues K402 and K420 are also located at one edge of the lipid exposed helix face. However, these residues mark the ends of the helix, and are sufficiently close to the polar/nonpolar boundary of the bilayer that the length of the lysine side chain would permit them to reach an environment where favorable solvation could be achieved.

The insertion of residues 402–420 in the bilayer as a transmembrane helix is in accord with the nearly complete protection of the membrane bound form of colicin from proteases demonstrated for colicin E1 (Zhang & Cramer, 1992) and Ia (Mel et al., 1993). However, it should be noted that current models for these colicins bound to membranes at zero transmembrane potential place helices other than VIII and IX parallel to the bilayer surface, with a transition of some or all helices to a transmembrane configuration upon application of a transnegative potential (Stroud, 1995; Qiu et al., 1996; Elkins et al., 1997). The data presented here suggest that Helix IV may populate a transmembrane configuration even at zero transmembrane potential, although this state may well be in equilibrium with one in which the helix lies parallel to the bilayer.

In summary, the SDSL/nitroxide scanning analysis of region 402–424 in colicin E1 in solution yields a structure entirely compatible with that determined for the crystal state of the C-terminal domain. In particular, both mobility and accessibility data reveal the presence of a regular helical structure from 406–416, corresponding to Helix IV in the crystal. Upon membrane binding, dramatic rearrangements in structure occur leading to a growth of Helix IV to include residues from 402–420 and disappearance of Helix Va. Concomitantly, the structure undergoes an effective inversion, with sites previously buried in the protein interior now exposed to the interior of the lipid bilayer on one face of the helix. The opposing face of the new helix is involved in interactions with the remainder of the protein, but in a manner that permits significant motion of side chains and apparently penetration of water at the contact sites. Depth analysis of the spin labeled side chains on the lipid-exposed surface of the helix favor a transmembrane orientation of the helix, at least for some fraction of the population. However, reversible pH dependent changes in the membrane bound structure raise the possibility that this state may be but one in a manifold of equilibrium states. Future SDSL studies of pH and voltage-dependent effects will be undertaken to characterize such equilibria, and elucidate the reversible channel gating event.

Materials and methods

Preparation of colicin E1 mutants

Constructs expressing mutant colicin E1 were prepared using PCR methods. An initial construct was prepared by subcloning a fragment of Col E1 Amp plasmid (Sigma, St. Louis, Missouri), corresponding to positions 4760–507 (NCBI ID 144307), into the multicloning site of the pUC18 plasmid utilizing SacI and HindIII restriction sites introduced within 5′ and 3′ PCR primers, respectively. To prepare an initial cysteine-less pseudo-wild-type mutant, the single native Cys505 was replaced by alanine. Additionally, silent mutations were introduced to create unique restriction sites NheI, NsiI and XbaI overlapping Leu374, Ala415, and Leu428 codons, respectively.

Single cysteines were introduced sequentially at positions 402 to 424. Mutations localized close to the one of restriction sites were introduced using synthetic oligonucleotides overlapping both mutation and restriction sites. Otherwise the “splicing by overlap extension” procedure was used as described by Horton and Pease (Horton & Pease, 1991). Amplified portions of the gene encoding

the C-terminal domain of the protein were sequenced to confirm introduction of the cysteine codon and to avoid errors introduced by Taq polymerase.

Expression and purification of col E1 mutants

The protein was expressed in *Escherichia coli* JC103 cells. Cultures were grown in LB medium (10 g tryptone, 5 g yeast extract, 5 g NaCl/1 L) enriched with 5 mL of 20% glucose and containing 50 mg/L ampicillin. Thirty milliliters of an overnight culture were used to inoculate 1 L of LB medium at 37 °C. Colicin production was induced in the late log phase by addition of 250 μg/L mitomycin D. Cells were harvested by centrifugation 3–4 h after induction and resuspended in 30 mL of ice cold buffer B (50 mM sodium borate, 50 mM NaCl, 80 μL/L β-ME, pH 9.5). The cells were disrupted in a French press and the insoluble debris removed by centrifugation (27,000 *g*, 10 min). The supernatant was diluted to 80 mL with ice cold buffer B and loaded on a CM Sephadex C-50 (Pharmacia, Uppsala, Sweden) column (2.5 x 16 cm) equilibrated with buffer B. After extensive washing with the same buffer, the protein was step-eluted with 300 mM NaCl. Fractions containing colicin E1, identified by UV absorbance ($OD_{280} \gg 1.0$), were pooled, dialyzed overnight against buffer M (50 mM MOPS pH 7.0, 50 mM NaCl, 80 μL β-ME), and stored at −20 °C.

In vivo activity test

An overnight culture (2.5 mL) of colicin E1–sensitive *E. coli* 514 cells was mixed with 40 mL of soft LB agar, and 3 mL of the mixture were plated on LB plates. Aliquots (5 μL) of 5x serial dilutions made from a stock containing 13 μg/mL of colicin E1 were spotted on 4 mm filter paper disks placed on the surface of the agar. Activity of the colicin was defined as highest dilution resulting in a clear zone around a disk after 4 h incubation at 37 °C.

Preparation of the colicin E1 tryptic fragment

Freshly prepared trypsin solution (1 mg/mL, type XIII, Sigma, St. Louis, Missouri) was added to a colicin solution (typically 2.5 mL/mL in 10 mM MOPS, 1 M NaCl, pH 7.0) at a final colicin:trypsin ratio of 50:1 (w/w). The reaction was terminated after 5–8 h of incubation at room temperature by addition of 0.1 mg of immobilized trypsin inhibitor (Sigma, St. Louis, Missouri). The reaction mixture was concentrated to less than 0.5 mL on Microsep-10 (Filtron, Northborough, Massachusetts) concentrator and than diluted to 20 mL with 50 mM MES, pH 5.5 buffer containing 80 μL/mL β-ME and loaded on a ResourceS column (Pharmacia) equilibrated with the same buffer. The major product of proteolysis was eluted with a 5–200 mM NaCl gradient and identified by sequencing the first 5–6 N-terminal aminoacids (UCLA microsequencing facility).

Spin labeling of colicin E1

The cysteine substitution mutants of the colicin E1 tryptic fragment were modified with (1-oxyl-2,2,5,5 tetramethylpyrroline-3-methyl) methanethiosulfonate (I) using a modification of procedure described by Todd (Todd et al., 1989). Briefly, the protein was incubated for at least 3 h with 10 mM DTT. Excess DTT was removed on a PD-10 size exclusion column (Pharmacia), equilibrated with LS buffer (10 mM MOPS, 10 mM NaCl, 1 mM EDTA, 0.2% sodium azide, pH 7.0), and a 20x molar excess of (I) added. After an overnight incubation, the protein was separated from unreacted (I) on a PD-10 column equilibrated with HS buffer (10 mM MOPS, 150 mM NaCl, 1 mM EDTA, 0.2% sodium azide, pH 7.0), and the eluant concentrated on a Microsep-10 microconcentrator to a final protein concentration of 100–300 μM. The concentration of nitroxide in a sample was determined by double integration of the EPR spectrum using an aqueous nitroxide solution of known concentration as a standard. The concentration of colicin E1 fragment was determined from the UV absorbance at 280 nm ($\epsilon_{280} = 1.43\ (\text{mg/mL})^{-1}\ \text{cm}^{-1}$). The extent of spin labeling was computed from these values.

Preparation of liposomes

POPC, POPG, and SLPC-n (n = 7, 10, 12) were obtained from Avanti Polar Lipids (Alabaster, Alabama) and used without purification. A mixture of 50 mg of POPC and 25 mg of POPG in chloroform was purged with nitrogen until dry. If required, SLPC-n was added at this step at 500:1 (mol lipid:mol SLPC-n) ratio. Residual chloroform was removed by overnight incubation under vacuum. Dried lipids were hydrated with 350 μL of 50 mM formic acid buffer (pH = 3.5) containing 150 mM NaCl. Unilamellar liposomes were prepared by extrusion through 100 nm polycarbonate filters using LiposoFast extruder (Avestin, Ottawa, Canada).

Preparation of membrane bound colicin E1 tryptic fragment

The membrane bound colicin E1 fragment was prepared by mixing equal volumes of the above liposome suspension and colicin fragment (100–300 μM) in HS buffer. The final pH was 4.0 ± 0.1 and lipid:protein ratio was at least 500:1 (mol:mol).

To investigate the effect of pH changes on the membrane bound tryptic fragment, the sample prepared as above was mixed at 3:1 (vol:vol) ratio with 150 mM, MOPS 150 mM NaCl, pH = 7.6 buffer. The final pH was 7.1.

EPR measurements

Samples of 5 μL were loaded in a gas permeable TPX capillaries. All spectra were recorded at room temperature on Varian E-109 X-band spectrometer fitted with loop gap resonator (Hubbell & Hyde, 1987) using 2 mW incident microwave power and ca. 1 G modulation. Power saturation analysis under a nitrogen atmosphere, in the presence of O_2 in equilibrium with air and in the presence of NiEDDA (10 mM for colicin in solution and 150 mM for colicin bound to vesicles), was carried out as described previously (Altenbach et al., 1989).

Depth calibration

Depth calibration equation (Equation 2) was obtained using phosphatidylcholine having a spin label located at positions 7, 10, 12 along the sn-2 fatty acyl (SLPC-n, n = 7,10, 12). Φ values were measured for samples containing unlabeled colicin E1 and plotted against known immersion depth of the spin labels (Dalton et al., 1987). Parameters *a* and *b* of Equation 2 were obtained by linear regression.

Acknowledgments

We thank Drs. P. Elkins and C. Stauffacher for providing colicin E1 coordinates and L. Columbus for critical reading of the manuscript. This work was supported by NIH Grant EY05216 and the Jules Stein Professorship endowment. The authors are also grateful to the Bundy Foundation for their generous support.

References

Alber T, Sun DP, Nye JA, Muchmore DC, Matthews BW. 1987. Temperature-sensitive mutations of bacteriophage T4 lysozyme occur at sites with low mobility and low solvent accessibility in the folded protein. *Biochemistry 26*:3754–3758.

Altenbach C, Flitsch SL, Khorana HG, Hubbell WL. 1989. Structural studies on transmembrane proteins. 2. Spin labeling of bacteriorhodopsin mutants at unique cysteines. *Biochemistry* 28:7806–7812.

Altenbach C, Greenhalgh DA, Khorana HG, Hubbell WL. 1994. A collision gradient method to determine the immersion depth of nitroxides in lipid bilayers: Application to spin-labeled mutants of bacteriorhodopsin. *Proc Natl Acad Sci USA 91*:1667–1671.

Altenbach C, Marti T, Khorana HG, Hubbell WL. 1990. Transmembrane protein structure: Spin labeling of bacteriorhodopsin mutants. *Science 248*:1088–1092.

Bowie JU, Luthy R, Eisenberg D. 1991. A method to identify protein sequences that fold into a known three-dimensional structure. *Science 253*:164–170.

Collarini M, Amblard G, Lazdunski C, Pattus F. 1987. Gating processes of channels induced by colicin A, its C-terminal fragment and colicin E1 in planar lipid bilayers. *Eur Biophys J 14*:147–153.

Cramer WA, Heymann JB, Schendel SL, Deriy BN, Cohen FS, Elkins PA, Stauffacher CV. 1995. Structure-function of the channel-forming colicins. *Annu Rev Biophys Biomol Struct 24*:611–641.

Dalton LA, McIntyre JO, Fleischer S. 1987. Distance estimate of the active center of D-beta-hydroxybutyrate dehydrogenase from the membrane surface. *Biochemistry 26*:2117–2130.

Dankert JR, Uratani Y, Grabau C, Cramer WA, Hermodson M. 1982. On a domain structure of colicin E1. A COOH-terminal peptide fragment active in membrane depolarization. *J Biol Chem 257*:3857–3863.

Eisenberg D, Weiss RM, Terwilliger TC. 1984. The hydrophobic moment detects periodicity in protein hydrophobicity. *Proc Natl Acad Sci USA 81*:140–144.

Elkins P, Bunker A, Cramer WA, Stauffacher CV. 1997. A mechanism for toxin insertion into membranes is suggested by the crystal structure of the channel-forming domain of colicin E1. *Structure 5*:443–458.

Engelman DM, Steitz TA, Goldman A. 1986. Identifying nonpolar transbilayer helices in amino acid sequences of membrane proteins. *Annu Rev Biophys Biophys Chem 15*:321–353.

Farahbakhsh ZT, Altenbach C, Hubbell WL. 1992. Spin labeled cysteines as sensors for protein-lipid interaction and conformation in rhodopsin. *Photochem Photobiol 56*:1019–1033.

Feix JB, Klug CS. 1998. Site-directed spin labeling of membrane proteins and peptide-membrane interactions. In: Berliner LJ, ed. *Spin labeling. The next millennium*. New York: Plenum Press.

Freed J. 1989. In: Berliner JL, Reuben J, eds. *Spin labeling: Theory and applications*. New York: Plenum Press.

Geli V, Koorengevel MC, Demel RA, Lazdunski C, Killian JA. 1992. Acidic interaction of the colicin A pore-forming domain with model membranes of *Escherichia coli* lipids results in a large perturbation of acyl chain order and stabilization of the bilayer. *Biochemistry 31*:11089–11094.

Honig BH, Hubbell WL, Flewelling RF. 1986. Electrostatic interactions in membranes and proteins. *Annu Rev Biophys Biophys Chem 15*:163–193.

Horton RM, Pease LR. 1991. Recombination and mutagenesis of DNA sequences using PCR. In: McPherson MJ, Quirke P, Taylor GR, eds. *PCR, a practical approach*. Oxford: Oxford University Press.

Hubbell WL, Altenbach CA. 1994. Investigation of structure and dynamics in membrane proteins using site-directed spin labeling. *Curr Opin Struct Biol 4*:566–573.

Hubbell WL, Gross A, Langen A, Lietzow MA. 1998. Recent advances in site-directed spin labeling of proteins. *Curr Opin Struct Biol 8*:659–656.

Hubbell WL, McHaourab HS, Altenbach C, Lietzow MA. 1996. Watching proteins move using site-directed spin labeling. *Structure 4*:779–783.

Hubbell WLF, Hyde JS. 1987. Continuous and stopped flow EPR spectrometer based on a loop gap resonator. *Rev Sci Instrum 58*:1879–1886.

Jahnig F. 1983. Thermodynamics and kinetics of protein incorporation into membranes. *Proc Natl Acad Sci USA 80*:3691–3695.

Kienker PK, Qiu X, Slatin SL, Finkelstein A, Jakes KS. 1997. Transmembrane insertion of the colicin Ia hydrophobic hairpin. *J Membr Biol 157*:27–37.

Kim YV, Opella SJ, Schendel SL, Cramer WA. 1998. Solid-state NMR studies of the membrane-bound closed form of the colicin E1 channel domain in lipid bilayers. *Protein Sci 7*:342–348.

Klug CS, Su W, Feix JB. 1997. Mapping of the residues involved in a proposed beta-strand located in the ferric enterobactin receptor FepA using site-directed spin-labeling. *Biochemistry* 36:13027–13033.

Koteiche HA, Berengian AR, Mchaourab HS. 1998. Identification of protein folding patterns using site-directed spin labeling. Structural characterization of a beta-sheet and putative substrate binding regions in the conserved domain of alpha A-crystallin. *Biochem 37*:12681–12688.

Lambotte S, Jasperse P, Bechinger B. 1998. Orientational distribution of alpha-helices in the colicin B and E1 channel domains: A one and two dimensional 15N solid-state NMR investigation in uniaxially aligned phospholipid bilayers. *Biochemistry 37*:16–22.

McDermott G, Prince SM, Freer AA, Hawthornthwaite-Lawless AM, Papiz MZ, Cogdell RJ, Isaacs NW. 1995. Crystal structure of an integral membrane light-harvesting complex from photosynthetic bacteria. *Nature 374*:517–521.

Mchaourab HS, Lietzow MA, Hideg K, Hubbell WL. 1996. Motion of spin-labeled side chains in T4 lysozyme. Correlation with protein structure and dynamics. *Biochemistry 35*:7692–7704.

Mel SF, Falick AM, Burlingame AL, Stroud RM. 1993. Mapping a membrane-associated conformation of colicin Ia. *Biochemistry 32*:9473–9479.

Merrill AR, Cramer WA. 1990. Identification of a voltage-responsive segment of the potential-gated colicin E1 ion channel. *Biochemistry 29*:8529–8534.

Oh KJ, Zhan H, Cui C, Hideg K, Collier RJ, Hubbell WL. 1996. Organization of diphtheria toxin T domain in bilayers: A site-directed spin labeling study. *Science 273*:810–812.

Parker MW, Postma JP, Pattus F, Tucker AD, Tsernoglou D. 1992. Refined structure of the pore-forming domain of colicin A at 2.4 A resolution. *J Mol Biol 224*:639–657.

Perozo E, Cortes DM, Cuello LG. 1998. Three-dimensional architecture and gating mechanism of a K+ channel studied by EPR spectroscopy. *Nat Struct Biol 1998*:459–469.

Qiu XQ, Jakes KS, Kienker PK, Finkelstein A, Slatin SL. 1996. Major transmembrane movement associated with colicin Ia channel gating. *J Gen Physiol 107*:313–328.

Slatin SL, Qiu XQ, Jakes KS, Finkelstein A. 1994. Identification of a translocated protein segment in a voltage-dependent channel. *Nature 371*:158–161.

Song HY, Cohen FS, Cramer WA. 1991. Membrane topography of ColE1 gene products: The hydrophobic anchor of the colicin E1 channel is a helical hairpin. *J Bacteriol 173*:2927–2934.

Stroud R. 1995. Ion channel forming colicins. *Curr Opin Struct Biol 5*:514–520.

Timofeev VP, Samarianov BA. 1993. About a new universal approach to the EPR spectra simulation of the spin-labeled molecules. *Appl Magn Reson 4*:523–539.

Todd AP, Cong J, Levinthal F, Levinthal C, Hubbell WL. 1989. Site-directed mutagenesis of colicin E1 provides specific attachment sites for spin labels whose spectra are sensitive to local conformation. *Proteins 6*:294–305.

Vetter IR, Parker MW, Tucker AD, Lakey JH, Pattus F, Tsernoglou D. 1998. Crystal structure of a colicin N fragment suggests a model for toxicity. *Structure 6*:863–874.

Voss J, Hubbell WL, Hernandez-Borrell J, Kaback HR. 1997. Site-directed spin-labeling of transmembrane domain VII and the 4B1 antibody epitope in the lactose permease of Escherichia coli. *Biochemistry 36*:15055–15061.

Wiener M, Freymann D, Ghosh P, Stroud RM. 1997. Crystal structure of colicin Ia. *Nature 385*:461–464.

Xu S, Cramer WA, Peterson AA, Hermodson M, Montecucco C. 1988. Dynamic properties of membrane proteins: Reversible insertion into membrane vesicles of a colicin E1 channel-forming peptide. *Proc Natl Acad Sci USA 85*:7531–7535.

Zakharov SD, Lindeberg M, Griko Y, Salamon Z, Tollin G, Prendergast FG, Cramer WA. 1998. Membrane-bound state of the colicin E1 channel domain as an extended two-dimensional helical array. *Proc Natl Acad Sci USA 95*:4282–4287.

Zhang YL, Cramer WA. 1992. Constraints imposed by protease accessibility on the trans-membrane and surface topography of the colicin E1 ion channel. *Protein Sci 1*:1666–1676.